RSC Advances

ROYAL SOCIETY OF CHEMISTRY

www.rsc.org/advances

RSC Advances

ARTICLE

Controllable growth of organic nanostructures from 0D to 1D with different optical properties

Received 00th January 20xx,
Accepted 00th January 20xx

DOI: 10.1039/x0xx00000x

www.rsc.org/

Yusen Luo,[a] Zheng Xue,[a] YongjunLi,[b] HuibiaoLiu,[b] Wensheng Yang[a] and Yuliang Li[b]

Two donor-π-donor (D-π-D) type compounds containing carbazole as the electron donor around the perylene core were synthesized and fabricated into controllable nano/microstructures from 0D to 1D by adjusting the growth rate. The difference in symmetry between two molecules results in distinct self-assembly behaviours. Fluorescence microscopy images and fluorescence spectra of these self-assembled structures displayed different optical properties. It is indicated that the photophysical properties of these twp compounds in solid states are determined not only by their chemical structures but also by the mode of molecular packing.

Introduction

Nanomaterials have received a rapid development by virtue of their excellent properties varied from their individual components[1, 2]. To date, a great number of inorganic and organic materials are used to prepare nano-sized structures with desired size and shape through "top-down" and "bottom-up" methods[3-6]. Among them, organic nanomaterials with well-defined structures and novel functions have aroused much attention because of their potential applications in photonic and electronic fields[7-9]. Utilizing intermolecular forces to construct such nanostructures through self-assembly of low-weight organic molecules are facile and valid methods to realize expected functions. This bottom-up technique offers possibility to tune the functions of solid materials at the molecular level.

Intermolecular forces, apart from commonly hydrogen bonding[10], π-π stacking[11] and electrostatic interaction[12], dipole-dipole interaction is also used to drive self-assembly especially in the intramolecular charge-transfer (ICT) compounds which are highly polarized[13]. This directional supramolecular interaction has recently been used to induce the growth of low-dimensional such as 1D or semi-1D organic nanostructures[14, 15]. Nanomaterials composed of ICT compounds are of great importance due to their fascinating applications in dye-sensitized solar cells[16], sensors[17], information storage materials[18], nonlinear optical materials[19], etc. Reasonable designed ICT compounds with controlled self-assembly processes are hot topics for novel applications in the future.

The design of ICT compounds based on carbazole as the donor with various aggregate nanostructures and properties have been widely investigated[20-22]. However, controlling the self-assembly processes in order to adjust the dimensionality of nanostructures and clarifying the structure-property relationships are still challenging. Here, we report on design strategies and structure-property studies for self-assembly of conjugated compounds based on carbazoles. Asymmetric and symmetric compounds were synthesized through changing the number of carbazole units around the perylene core. The difference on the molecular symmetry can lead to the polarization of the molecules. Then supramolecular aggregates with 0D and 1D structures were obtained from these compounds by tuning the growth rate. Finally optical properties of these nanostructures were also investigated in order to clarify the structure-property relationships.

Results and discussion

The synthesis of target molecules **TBC** and **TCP** (Figure 1) is shown in Scheme S1. Details of the experiments are described in the Experimental section. In brief, we obtained two molecules with different symmetry by adjusting the number of carbazole units. It is important to note that the asymmetric **TBC** has additional dipole-dipole interaction between molecules except the evident π-π interaction as dominated in **TCP**.

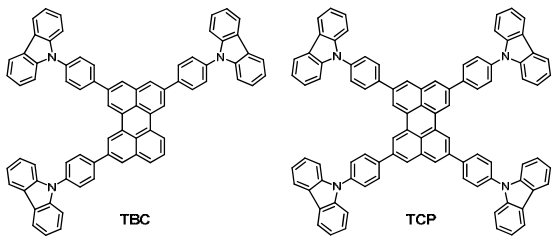

Figure 1. Molecular structures of **TBC** and **TCP**.

[a] *State Key Laboratory for Supramolecular Structures and Materials, College of Chemistry, Jilin University, Changchun 130012, P. R. China. E-mail: wsyang@jlu.edu.cn; Fax: +86-431-85168186; Tel: +86-431-85168185*
[b] *CAS Key Laboratory of Organic Solids, Beijing National Laboratory for Molecular Science (BNLMS), Institute of Chemistry, Chinese Academy of Sciences, Beijing, P. R. China. E-mail: liyj@iccas.ac.cn; Fax: +86-10-82616576; Tel: +86-10-82615870*
†Electronic Supplementary Information (ESI) available: See DOI: 10.1039/x0xx00000x

Electrochemical properties

The electrochemical properties of **TBC** and **TCP** were studied by cyclic voltammetry (CV) and differential pulse voltammetry (DPV) at room temperature in dichloromethane solution. Both CV curves showed only two pairs of irreversible oxidation waves which indicated the two compounds are more like the donor-π-donor (D-π-D) type rather than D-π-A. The irreversible processes are related with the oxidation steps of carbazole[20] and perylene[23]. Due to the irreversible electrochemical processes, DPVs were tested and ferrocene was used as internal standard substance in order to calculate the HOMO energies[24, 25] (Figure S1b, d, Table 1). For **TBC**, the first oxidation potential (E_1^{ox}) is 0.57 V, the second oxidation potential (E_2^{ox}) is 0.84 V. Compared with **TBC**, the E^{ox} values of **TCP** showed a slight positive shift of about 0.02 V (E_1^{ox}= 0.59 V, E_2^{ox}= 0.86 V) which might be result from the stronger electron-push group[26] in **TCP**.

Photophysical properties

UV-Vis and fluorescence spectra are very sensitive to the intermolecular distance and orientation, therefore the interaction between molecules could be reflected from them to some extent. Figure 2a shows the normalized UV-Vis absorption spectra of **TBC** and **TCP** in CH_2Cl_2 solution (1×10^{-5} M) and cast films. The spectral parameters are summarized in Table 1. Four distinct UV-Vis absorption bands were observed in both of them and the bands at around 290 nm would be associated with the π-π* transition of the carbazole units[27] in two molecules. Three bands in visible region could be assigned to the π-π* transition in perylene core[28]. From Figure 2a, it is revealed that the absorption bands would experience red shift as the π- conjugated systems become longer and the electron donors become stronger[29, 30].Just as the maximum absorption band had a red shift of 8 nm as the **TCP** has longer conjugated system and stronger electron donors. Furthermore, the absorption band of **TBC** film presented an obvious red shift of 11 nm compared with its diluted solution, which indicates the formation of J-type aggregates and π – π interactions among neighbouring molecules in solid states[11, 31]. With regard to compound **TCP**, the absorption spectrum of film became structureless and with a red shift compared to that in solution. It means that compound **TCP** would also form the J-type aggregates in solid states. The long tail absorption of **TCP** solids might result from the scattering of some microparticles in the film, which at the same time could affect the light transmittance thus the structureless absorption band and low absorbance was obtained (Figure S2). From the onset of absorption spectra, E_g^{opt} of 2.70 eV and 2.59 eV were obtained for **TBC** and **TCP**, respectively. Thus LUMO energy levels of -2.27 eV and -2.40 eV were derivated for **TBC** and **TCP**.

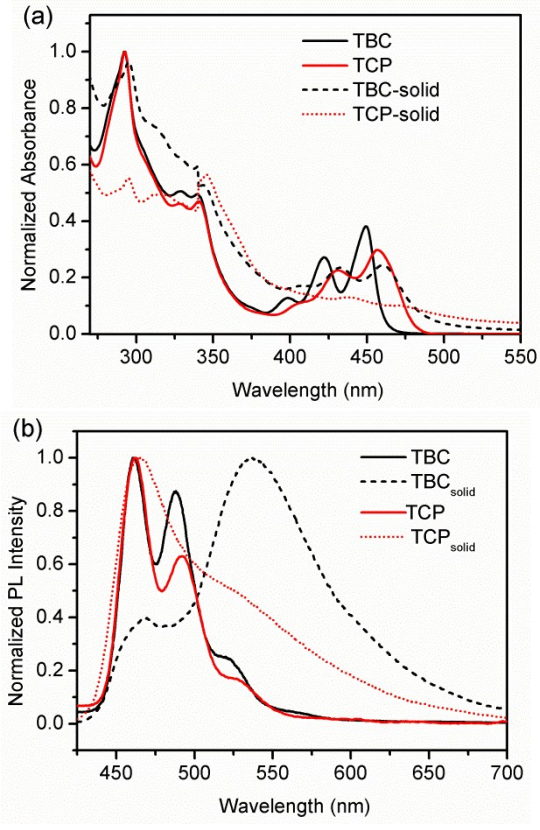

Figure 2.(a) Normalized UV-Vis absorption spectra of the ICT compounds in CH_2Cl_2 solution (1×10^{-5} M) and solid states. (b) Normalized PL emission spectra both in solution and solid states. The excitation wavelengths used were 398 nm and 405 nm for **TBC** and **TCP** respectively.

Table 1. Photophysical properties and calculating data of **TBC** and **TCP**.

COMPD	$\lambda^{abs}{}_{max}$(nm) (log ε) [a]	λ_{em}(nm)[b]	Φ_{fl} [c]	HOMO[d] /LUMO[e] (eV)	E_g [f] (eV)
TBC	398(4.45), 421(4.79), 449(4.93)	461,488,522	0.90	-4.97,-2.27	2.70
TCP	405(4.06), 430(4.37), 457(4.48)	462,492,528	0.85	-4.99,-2.40	2.59
TBC$_{film}$	406, 432, 460	467,537	\	\	\
TCP$_{film}$	438, 473	465,524	\	\	\

[a, b] Measured in 1×10^{-5} M CH_2Cl_2 solution. [b]**TBC** and **TCP** was excited at 398nm and 405 nm respectively. [c]In CH_2Cl_2, Quinine sulfate dihydrate, Φ_{fl} = 0.53 in 0.1 M H_2SO_4 as the standard. [d]HOMO energies were calculated by the onset oxidation potential. HOMO = -e (E_{ox}^{onset} + 4.40) eV. [e]LUMO energies were calculated through the formula: E_g = LUMO-HOMO. [f]E_g was obtained from the onset of absorption spectra according to E_g = 1240/ λ.

Fluorescence spectra of **TBC** and **TCP** were also recorded in the two states and both molecules gave intense fluorescence in solution and films (Figure 2b). The emission spectra of solution are well mirror images with respect to their absorption bands. The maximum emission band of **TBC** monomers was located at 461 nm with two shoulders (488nm, 522 nm) when excited at 398 nm.. The solution of **TCP** gives PL centred at 462 nm with two shoulder peaks at 492 and 528nm when excited at 405 nm. The Stokes' shifts of **TBC** and **TCP** were very small (Δλ = 12 nm, 5 nm respectively) and their fluorescence quantum yields were given in Table 1. It is interesting to note that the emission spectra in solid states displayed different trends. For example, **TBC** film showed a broad red-shifted band having a maximum at 537 nm with a minor monomer emission around 467 nm. The minor band could be assigned to the shortest 0-0 transition observed in fluorescence spectrum in solution and the decrease in intensity was thought to originate from two factors : One is as a result of self-absorption according to literatures which also have small Stokes' shift[32], and the other is due to the number of individual molecules existing in the film decreased[33]. In addition, the broad red-shifted band was due to the perylene excimer which was usually observed in other's

work[31, 34, 35].Whereas the **TCP** film displayed a very prominent monomer emission locating at 465 nm and a relative weak, structureless emission band in the longer wavelength range. This observation indicates that in solid states, perylene core in **TCP** compounds would not or there were a very small amount of perylene molecules interact with neighbouring perylene on the excited states. This might be derived from its intrinsic molecular structures. That is there are four carbazoles around the perylene core which could cause less coplanar to the whole molecules. Together with the steric repulsion, it is mainly for carbazoles to interact with each other in solid states rather than perylene molecules. Thus the perylene excimer would not appear under this condition. Above results suggested that though both molecules formed a J-type stacking in solid states, there would be difference on their microstructure. As a consequence we could obtain various aggregate nanostructures with different optical properties through tuning parameters such as solvent and growth rate during the self-assembly processes. Detailed data are shown in Table 1.

Self-assembly and optical properties

Self-assembly is a valid method to construct organic nanostructures with high efficiency in no need of templates. It is important to note that the growth rate plays a key role in self-assembly in order to obtain nanostructures with desirable shape and size. In the following work, we adopted two pathways namely solvent vapor technique[36] and phase transfer methodology[37] to fabricate the ICT compounds into various nano/microstructures from 0D to 1D by adjusting the growth rate. The initial concentration (1×10^{-3} M) of both molecules was kept the same.

The solubility of **TBC** and **TCP** is "good" in dichloromethane and tetrahydrofuran but "poor" in hexane, methanol and acetone. By solvent vapor technique, compound **TBC** could self-assemble into sphere-like architectures. Injection of poor, same volume of hexane into a solution of **TBC** in CH_2Cl_2 with sufficient stirring, after solvent evaporated, a certain structure of aggregates was obtained. As shown in scanning electron microscopy (SEM) and transmission electron microscopy (TEM) images (Figure 3a, b), nanospheres with an average diameter of 500 nm were formed and TEM image further confirmed that the nanospheres had hollow morphology. It is expected that during the solvent evaporation process, **TBC** molecules segregated from CH_2Cl_2 should have been organized by intermolecular interactions to form definite structures in hexane after the good solvent evaporated firstly. The hollow nanospheres, or called vesicles are also obtained in other systems such as the amphiphilic perylene bisimide dyes[33, 38, 39]. The self-assembled nanostructures would undergo various shapes as a result of the different solvent polarity which can affect the shape and size of the formed micelles. However, in our work, the hollow-shaped nanostructures can form even if adjusting the solvent polarity (THF/CH_3OH). It is suggested that though the carbazole units have a certain hydrophilic property, it is not enough to be affected by the solvent polarity. Thus the mechanism of this process would be attributed to the certain directional molecular stacking and its relevant growth rate (Figure 3g, 4 g).

With the same mixture solvents CH_2Cl_2 / hexane, slowing down the growth rate of **TBC** molecules during self-assembly, one-dimensional nanotubes were formed. The operation process is described as follows: adding poor solvent hexane slowly to the CH_2Cl_2 solution with the volume ratio of 4:1, 1D nanotubes were obtained as yellow precipitates after the mixture placed for five days without disturbance. SEM and TEM images (Figure 3d, e) showed that the nanotubes were well monodispersed with an average width of 100 nm and length up to several micrometers. Under this condition, nucleation first happened at the interface between two solvents followed by the slow growth process of **TBC** molecules and finally well-defined nanotubes were formed by synergistic effect of different intermolecular forces (Figure 3g). The possible mechanism for the morphology transition was proposed as a "curvature strain releasing" process driven by donor-acceptor dipole-dipole interactions[40].

Fluorescence microscopic images (Figure 3c, f) of **TBC** in 0D and 1D supramolecular architectures were totally different. Both structures were intense emitters and for nanospheres, they radiated strong yellow fluorescence but for the nanotubes, green fluorescence was observed. It is interesting to note that, for the same compound, we could control the dimensionality of nanostructures from 0D to 1D just by adjusting their growth rate and these nanostructures would own disparate optical properties.

For compound **TCP**, large-scale spheres measuring several hundred nanometers (800-1000 nm) were observed by solvent vapor technique (Figure 4a). TEM images (Figure 4b) also indicated these nano/microspheres were hollow structures. Morphology transition was also observed when slowing down the growth rate by phase transfer methodology. Figure 4d shows typical SEM image of nanorods with width of about 760 nm and TEM image (Figure 4e) further indicated they were solid structures with length up to several micrometers (Figure 4g). The parameters of self-assembly processes namely the operation method, solvent, initial concentration of ICT compounds, volume ratio were the same as that of **TBC** described above. Fluorescence microscopic images (Figure 4c, f) were taken to investigate the morphologies and fluorescence emission of nano/microsphere and nanorods. Interestingly, in contrast with **TBC** molecules, the different supramolecular structures of **TCP** showed similar emission behaviour, both were yellow fluorescence.

In order to compare the optical properties of various nanostructures directly, their corresponding fluorescence spectra were recorded (Figure 5). For **TBC** and its relevant self-assembled structures, the maximum emission bands of nanospheres and nanotubes both experienced red-shift compared with molecules in solution but differing in degree (Figure 5a). In accordance with the fluorescence microscopic images, these two kinds of morphologies had different illuminant property. The λ_{em} of nanotubes red-shifted from 488 nm in solution to 519 nm while the λ_{em} of nanospheres red-shifted much more to 545 nm. As said before, the broad red-shifted band was attributed to the excimer emission. This emission band of nanospheres is more red-shifted and broader than that of nanotubes, which means better exciton migration originating from stronger π –π interaction among perylene cores but less well-organized molecules aggregation in spherical structures[33, 35]. Thus, the microstructures within nanospheres and nanotubes are different, which would in turn affect the optical properties of solid materials.

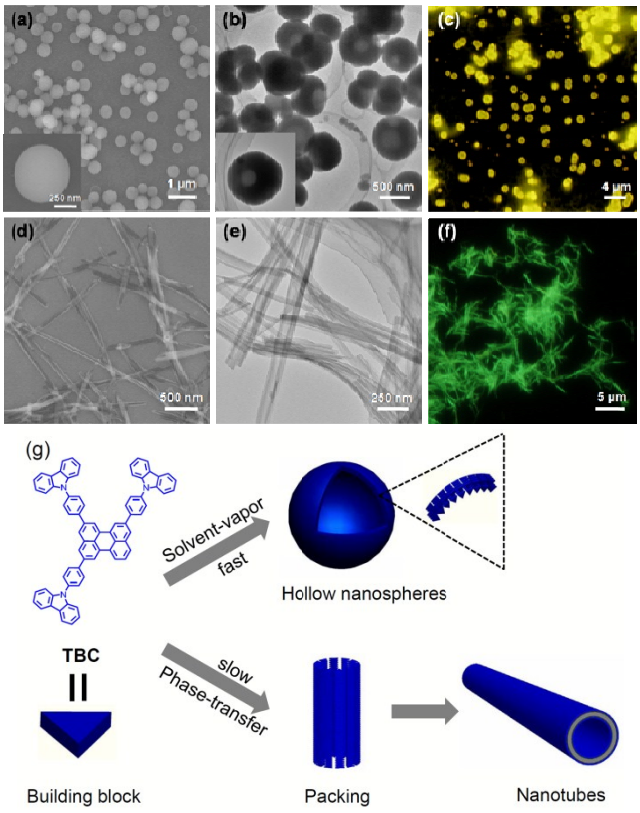

Figure 3.SEM, TEM and corresponding fluorescence microscopic images (excited by a UV band (330–380 nm) light source) of self-assembled nanospheres (a-c) and nanotubes (d-f) of **TBC**. Note: for the different techniques, same poor and good solvents were used. The difference in morphologies would mainly be result from the growth rate. (g) The proposed mechanism for the self-assembly of **TBC**.

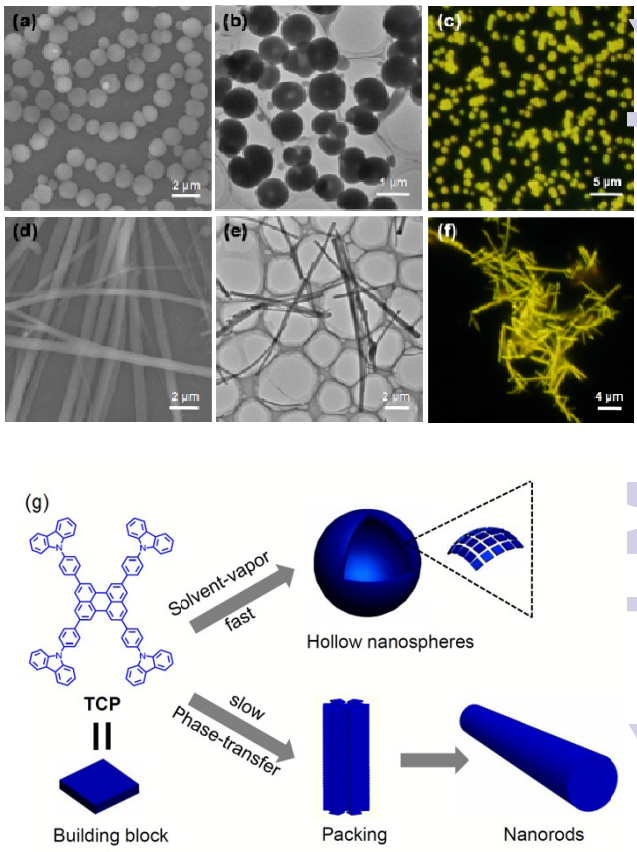

Figure 4. Large-area SEM and TEM images of self-assembled **TCP**: nanospheres (a-b) and nanotubes (d-e).The corresponding fluorescence microscopic images (c, f) show the similar emission property of both nanostructures. (g) The proposed mechanism for the self-assembly of **TCP**.

Meanwhile the fluorescence spectra of nanostructures of **TCP** showed the same results as displayed in the fluorescence microscopic images. The shape of the bands and λ_{em} of nano/microspheres and nanorods were nearly the same (~464 nm) only with a little difference in the region between 530 nm and 580 nm (Figure 5 b). According to the previous study (Figure 2b), it is difficult for perylene units to interact with each other on excited states, which was in accordance with the unconspicuous excimer emission bands here. However, the π –π interaction among perylenes thus excitonic coupling are stronger in nanorods, which can be deduced from the emission spectra between 530 nm and 580 nm in Figure 5 b and also in Figure 4 g. To form the rod-shaped nanostructures, **TCP** moelcules should be packed more tightly than those in hollow nanospheres, therefore the probability of interaction among perylenes was increased. The results demonstrated that the optical properties of organic supramolecular aggregates are not only related to the molecular structure itself (compared with **TBC** and **TCP**), but also has relationships with the molecular packing in solid states (when compared the same compounds of different shapes).

At this stage, we acquired self-assembled nanostructures of **TBC** and **TCP** with controllable shapes and dimensionality, namely nano/microspheres, nanotubes and nanorods which have high morphologies purity without other kinds of structures. It has been discussed that for the same compounds, 0D to 1D nanostructure could be formed by tuning the growth rate. As can be seen from the above results, the properties (electrochemistry, absorption and fluorescence spectra) of **TBC** and **TCP** in solution have very subtle difference. However, the optical properties have considerable difference once they were fabricated into self-assembled nanostructures, which would be attributed to the various molecular packing in solid states.

It is interesting to note that the difference in chemical structures of symmetry would result in rather distinct self-assembly behaviour and distinct optical properties under the same conditions. **TCP** has very symmetric structure and dipole moments from all directions are offset. The major driving force for formation of nanostructures is the π-π interaction. However, for **TBC**, it is asymmetric and the vector resultant force of dipole from several directions would be the driving force. Thus there were mainly two kinds of intermolecular forces, π-π and dipole-dipole interactions, would induce molecules to form certain structures under different environments. In solvent vapor technique, although spherical structures were obtained for both compounds, the molecular packing was largely different. This can be reflected from the emission spectra (Figure 5 a-b) that both nanospheres had two emission bands at around 465 nm (monomer emission) and 545 nm (excimer emission) but differed in relative intensity. The different

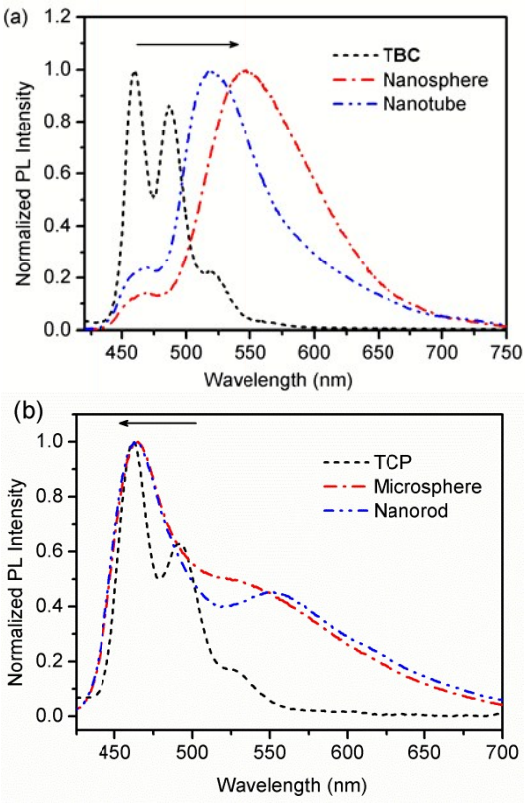

Figure 5. Normalized PL emission spectra of **TBC** (a) and **TCP** (b) molecules both in solution and in the self-assembled aggregates states. They were excited at 398 nm and 405 nm respectively.

molecular packing during self-assembly resulted in different size (Figure 3g, 4g). Difference between **TBC** and **TCP** compounds became more obvious in phase transfer methodology which has slower growth process. That is **TBC** could be fabricated into tube-like structures with green fluorescence while **TCP** could self-assembled into rod-like structures with yellow fluorescence.

Additionally, it is found that in solvent vapor technique, acetone as a poor solvent could induce totally different self-assembly results between **TBC** and **TCP**. The symmetric **TCP** would produce 2D flower-like structures when little amount of acetone added, however, the asymmetric **TBC** could not form similar structures no matter how to tune the amount of acetone (see Supporting Information, Figure S3). The growth of **TCP** was carried out in CH_2Cl_2 / acetone (v/v, 40:3) by solvent vapor technique and large scale of microflowers bearing series of nanowires were obtained (Figure 6a, arrows). It is clearly to see that some microflowers only composed of a few nanowires while others displayed hierarchical structures with a large number of nanowires stacked together (Figure 6a, b). The inset in Figure 6b confirmed that the branches of microflowers were not smooth which were pod-like with many spheres fusing together. The microflowers also displayed strong yellow emission as other nanostructures of **TCP**. TEM images (Figure 6d-f) further confirmed that these microflowers were composed of nanowires which might be formed by fusing of primary nanospheres at certain directions.

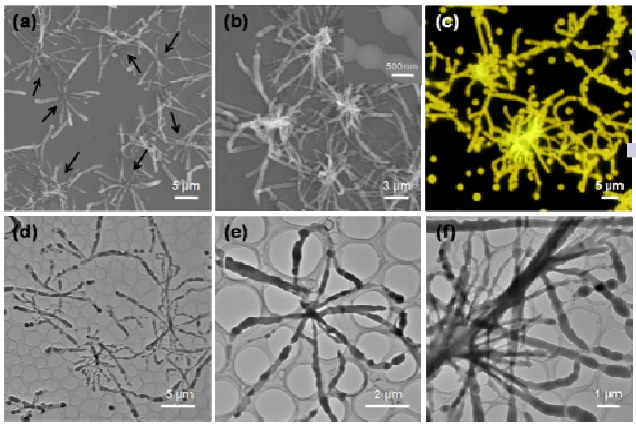

Figure 6.SEM (a, b) and TEM (d-f) images of **TCP** prepared in CH_2Cl_2/ acetone (40:3) by solvent vapor technique at room temperature. Figure (e) shows one microflower with simple structures and (f) shows one typical microflower with hierarchical structures. The corresponding fluorescence microscopic image(c) was also taken to examine the morphologies and fluorescence emission of flower-like structures.

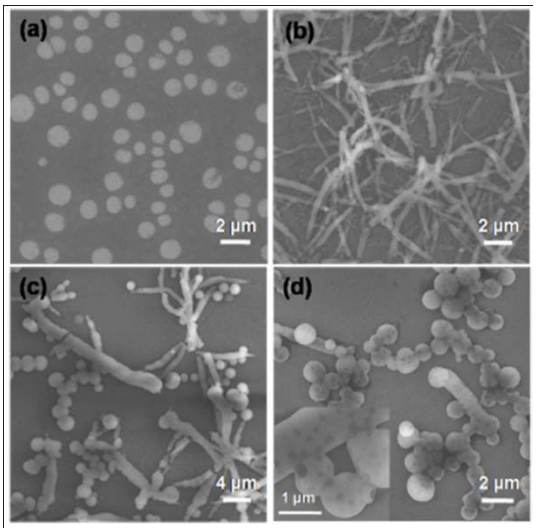

Figure 7.SEMimages of **TCP** prepared in CH_2Cl_2/ acetone with different volume ratio (v/v) by solvent vaportechnique. (a) v/v = 40:0, (b) v/v = 40:10, (c) v/v = 40:15 and (d) v/v = 40:40.

To clarify the role of acetone during this process, different amount of acetone was added to direct self-assembly of **TCP** molecules. Direct evaporating CH_2Cl_2 without acetone, quasi-spheres were formed with the diameter of nearly 500~1000 nm (Figure 7a). When increasing the amount of acetone to the volume ratio of 40:10, microflowers appeared but more unordered (Figure 7b). It was shown in Figure 6 that there were some nanospheres (about 500~1000 nm) dispersed around these microflowers with the same size as the width of branches. We proposed that at first stage, small nanospheres were appeared. Then the existing little amount of acetone could induce these nanospheres to fuse together forming the nanowires which would further connect together to form the final microflowers.

However, further increasing acetone to reach the volume ratio of 40:15, as shown in Figure 7c, nanorods combined with nanospheres were obtained with nearly the same proportion.

When the volume ratio reached 40:40, plenty of nanospheres were formed with some open holes on their surface (inset in Figure 7d) and these nanospheres were connected together seriously (Figure 7d), which is due to the fact that the large amount of acetone functions as the "poor" solvent in these cases. The results indicated that acetone could induce molecules of **TCP** to form 2D flower-like hierarchical structures when a little amount was added. Further increasing acetone would not produce such microstructures but result in nanospheres.

Conclusions

In summary, two donor-π-donor (D-π-D) type compounds containing carbazole as the electron donor around the perylene core were synthesized and fabricated into well-defined and controllable nanostructures. It is found that the dimensionality of the self-assembled nanostructures could be tuned from 0D to 1D just changing the growth rate. It is reasonable to conclude that the optical properties of organic nanomaterials are not only related to their molecular structures, but also have relationships with modes of molecular packing in solid states.

Acknowledgements

This work was supported by the National Natural Science Foundation of China (21290190, 21322301, 20803029, 51072064) and the National Basic Research 973 Program of China(2011CB935800, 2012CB932900), and the "Strategic Priority Research Program" of the Chinese Academy of Sciences(XDA09020302).

Notes and references

1 Y. Guo, L. Xu, H. Liu, Y. Li, C. Che and Y. Li, *Adv. Mater.*, 2015, **27**, 985-1013.
2 M. Safont-Sempere, G.Fernández and F. Würthner, *Chem.Rev.*, 2011, **111**, 5784-5814.
3 Y. Fernandez, T. Gschneidtner, C.Wadell, L. Fornander, S. Avila, C. Langhammer, F. Westerlund and K. Moth-Poulsen, *Nanoscale*, 2014, **6**, 14605-14616.
4 H. Yu, M. Regulacio, E. Ye and M. Han, *Chem. Soc. Rev.*, 2013, **42**, 6006-6018.
5 X. Li, Y. Ma, L. Qin, Z. Zhang, Z. Zhang, Y. Zhang and Y. Qu, *J. Mater. Chem. A*, 2015, **3**, 2158-2165.
6 R. Huang, Y. Wang, W. Qi, R. Su and Z. He, *Mater.Lett.*, 2014, **128**, 216-219.
7 Y. Li, T. Liu, H. Liu, M. Tian and Y. Li, *Accounts Chem.Res.*, 2014, **47**, 1186-1198.
8 Y. Yan and Y.Zhao, *Chem. Soc. Rev.*, 2014, **43**, 4325-4340.
9 L. Zang, Y.Che and J.Moore, *Accounts Chem.Res.*, 2008, **41**, 1596-1608.
10 L. Zhang, Y. Long, Z. Chen and M. Wan, *Adv. Funct. Mater.*, 2004, **14**, 693-698.
11 C. Huang, L. Wen, H. Liu, Y. Li, X. Liu, M. Yuan, J. Zhai, L. Jiang and D. Zhu, *Adv. Mater.*, 2009, **21**, 1721-1725.
12 T. Tsai, G. Heckert, L. Neves, Y. Tan, D. Kao, R. Harrison, D. Resasco and D. Schmidtke, *Anal. Chem.*, 2009, **81**, 7917-7925.
13 J. Xu, L. Wen, W. Zhou, J. Lv, Y. Guo, M. Zhu, H. Liu, Y. Li and L. Jiang, *J. Phys. Chem. C*, 2009, **113**, 5924-5932.
14 X. Zhang, X. Zhang, K. Zou, C. Lee and S. Lee, *J. Am. Chem. Soc.*, 2007, **129**, 3527-3532.
15 T. Liu, Y. Yu, S. Chen,Y. Li and H. Liu, *RSC Adv.*, 2013, **3**, 9973-9977.
16 S. Ito, H. Miura, S. Uchida, M. Takata, K. Sumioka, P. Liska, P. Comte, P. Pechyb and M. Gratzel, *Chem. Commun.*, 2008, **41**, 5194-5196.
17 Q. Li, M. Peng, H. Li, C. Zhong, L. Zhang, X. Cheng, X. Peng, Q. Wang, J. Qin and Z. Li, *Org. Lett.*, 2012, **14**, 2094-2097.
18 Y. Shang, Y. Wen, S. Li, S. Du, X. He, L. Cai, Y. Li, L. Yang, H. Gao and Y. Song, *J. Am. Chem. Soc.*,2007, **129**, 11674-11675.
19 J. Xu, S. Semin, D. Niedzialek, D.Niedzialek , P. Kouwer , E.Fron, E.Coutino , M.Savoini , Y. Li , J.Hofkens , H.Uji-I , D.Beljonne, T.Rasing and A. Rowan, *Adv. Mater.*, 2013, **25**, 2084-2089.
20 S. Chen, Z. Qin, T. Liu, X. Wu, Y. Li,H. Liu,Y. Song and Y. Li, *Phys. Chem. Chem. Phys.*, 2013, **15**, 12660-12666.
21 X. Sun, Y. Liu, X. Xu, C. Yang, G. Yu, S. Chen, Z. Zhao, Y. Qiu, Y. Li, and D. Zhu, *J. Phys. Chem. B*, 2005, **109**, 10786-10792.
22 D. Jiang, Z. Xue, Y. Li, H. Liu and W. Yang, *J. Mater. Chem. C*, 2013, **1**, 5694-5700.
23 A. Aleshinloye, J. Bodapati and H. Icil, *J Phptoch Photobio. A*, 2015, **300**, 27-37.
24 T. Johansson, W. Mammo, M. Svensson, M. Andersson and O. Ingana, *J. Mater. Chem.*, 2003, **13**, 1316-1323.
25 Y. Li , Y. Cao , J. Gao , D. Wang , G. Yu and A. Heeger, *Synthetic Met.*, 1999, **99**, 243-248.
26 S. Chen, Y. Li, W. Yang, N. Chen, H. Liu, and Y. Li, *J. Phys. Chem. C*, 2010, **114**, 15109-15115.
27 H. Zhang, X. Wan, X. Xue, Y. Li, A. Yu and Y. Chen, *Eur. J. Org. Chem.*, 2010, **9**, 1681-1687.
28 L. Zhao, W. Yang, Y. Ma, J. Yao, Y. Li and H. Liu, *Chem. Commun.*, 2003, **19**, 2442-2443.
29 Y. Zhu, A. Kulkarni, P. Wu and S. Jenekhe, *Chem. Mater.*, 2008, **20**, 4200-4211.
30 K. Chen, Y. Hsu, Q. Wu, M. Yeh and S. Sun, *Org. Lett.*, 2009, **11**, 377-380.
31 H. Wu, L. Xue, Y. Shi, Y. Chen and X. Li, *Langmuir*, 2011, **27**, 3074-3082.
32 A. Iida and S. Yamaguchi, *Chem. Commun.*, 2009, **21**, 3002-3004.
33 B. Jiang, D. Guo and Y. Liu, *J. Org. Chem.*, 2010, **75**, 7258-7264.
34 D. Das, G. Sahoo, P. Mazumdar, A. Maity, D. Chattopadhyay, G. Morán and A. Misra, *J. Mol. Liq.*, 2015, **206**, 47-55.
35 Y. Che, X. Yang, S. Loser and L. Zang, *Nano Lett.*, 2008, **8**, 2219-2223.
36 T. Liu, Y. Li, Y. Yan, Y. Li, Y. Yu, N. Chen, S. Chen,C. Liu, Y. Zhao and H. Liu, *J. Phys. Chem. C*, 2012, **116**, 14134-14138.
37 S. Chen, N. Chen, Y. Yan, T. Liu, Y. Yu, Y. Li,H. Liu, Y. Zhao and Y. Li,*Chem. Commun.*, 2012, **48**, 9011-9013.
38 X. Zhang, S. Rehm, M. Safont-Sempere and F. Würthner, *Nat. Chem.*, 2009, **1**, 623-629.
39 X. Yang, X. Xu and H. Ji, *J. Phys. Chem. B*, 2008, **112**, 7196-7202.
40 J. Xu, X. Liu, J. Lv, M. Zhu, C. Huang, W. Zhou, X. Yin, H. Liu, Y. Li, J. Ye, *Langmuir,* 2008, **24**, 4231–4237.